



PRECONDITIONING EFFECT ON SEM CONCRETE SAMPLES AND ITS IMPACT ON THE IMPLEMENTATION OF CONCRETE SURFACE ANALYSIS AT MICROSCOPIC SCALE

T. Chlayon¹ M. Iwanami¹ N. Chijiwa¹

¹ Tokyo Institute of Technology, Tokyo, Japan

ARTICLE INFO:

Received: July 15, 2018

Received Revised Form:

August 29, 2018

Accepted: September 3, 2018

ABSTRACT:

To date, the literature on micro-scale concrete has been actively conducted. Scanning electron microscopy (SEM) is widely used not only for microscopic inspections but also on-the-fly elemental identification. However, prior to SEM, the precondition of concrete specimen is necessary. This included drying the samples in a vacuum heater which later on led to a significant alternation of microscale concrete surface. Consequently, the representative SEM images, therefore, might not reflect the actual condition. Also, coating by conductive materials such as gold, platinum or palladium may have limitations regarding the surface deteriorations. This research investigated the SEM preconditioning effect on concrete samples by using four surface conditions: 1. regular, 2. rough by natural bleeding, 3. emulated erosion by applying sandpaper, and 4. acidic attack. The before and after preconditioning effects were inspected using an optical light-inverted microscope, while the SEM images were captured by JXA-8200, an electron probed microanalyzer (SEM-EPMA). In addition, the metallic coating using platinum (Pt) and palladium (Pd) regarding the four surface cases were discussed. Findings postulated an inconsistency of the conductive coating (Pt-Pd) among the four surfaces. Also, the vacuum-heating process did alter the microstructure of cement hydrate on concrete surface. Furthermore, a significant increment of microcracks was detected across the specimen surface at $\times 100$ magnification in all cases. Recently, the literature claimed that the concrete surface might have significant impacts on concrete properties and durability. This research might help in emphasizing the relationship between concrete surface and durability concerns such as weathering damage, and chloride attack.

**Corresponding Author,*

Email address:

Chlayon.t.aa@m.titech.ac.jp

KEYWORDS: SEM, concrete, surface, microcrack, image analysis

1. Introduction

For decades, scanning electron microscopy (SEM) has been implemented in the study of the concrete microstructure. Not only can this be used to perform a decent elemental analysis such as wave dispersive x-ray (WDX) and energy dispersive x-ray spectroscopy (EDS), but useful information regarding the surface condition of the concrete can also be acquired via scanning electron image (SEI) and back-scattered electron image (BEI). At present, a number of researchers in material and construction group have investigated durability issues of marine concrete [1]–[6], and certain researchers even utilized SEM in their study[7]–[12]. Due to the limitation, currently there are no substantial findings which indicated the concerns of the relationship between concrete durability and the surface condition, but this point was suspicious by several researchers mentioned in earlier. However, we also experienced issues in the investigation, because the SEM also has limited usage. To fully utilize the SEM, concrete and mortar samples inevitably need preconditioning. This procedure is utmost essential and significantly impacted any results obtained via SEM including both analysis data and visual image.

This paper investigated the before and after preconditioning effects prior to SEM analysis. We created four condition types of concrete surface that each of these represents different durability concerns. The light-inverted optical microscope was used to clarify the before and after preconditioning effects regarding the four surface types.

2. Material and Method

2.1 Mix design, sample preparation, and study cases

All samples were mortar, and the mix design was the same for all study cases. We used an ordinary Portland cement type I and a typical fine aggregate which is available in Japan. Fine aggregate had the density at the saturated-surface-dry of 2.63 g/cm³, and the fineness modulus was 2.38. The water to cementitious ratio, and the cement to aggregate ratio were 0.5, and 0.45 in order. No additional admixture was used.

All mortar specimens were cast using cylindrical molds; 50 mm in diameter by 100 mm in length. The bottom-side surface which was confined to the built-in steel end plate of the mold was selected for preparation of the Case 1, 3, and 4 specimens. As for the Case 2, the top-side surface was used because of naturally turning rough due to no surface confinement. One day after casting, all sample were de-molded and then placed in a curing tank in a 20-degree-Celsius temperature control chamber for 28

days. Later on, those specimens were cut into suitable size for the JXA-8200 tray (the SEM-EPMA analysis machine). The preparation was performed using a slow-speed cutter with lubricant oil. Both width and length of all samples were trimmed to less than 40 mm, and the thickness was approximately 5 mm. Finally, all samples were cleaned by oil and sapped dry by high-grade tissue papers.

Table 1 Temperature at the construction site

Case No.	Surface condition	Descriptions
1	Regular flat	Store in 20 °C temperature control room
2	Rough	Turn rough by natural bleeding
3	Abrasive force	Apply sandpaper No. 120 on surface
4	Acidic attack	Submerge in high concentration sulfuric acid solution for two days

Four surface conditions were prepared representing certain deterioration environments. They included the regular smooth surface, the rough surface caused by bleeding effect when casting without proper surface finishing, the surface under abrasion and erosion forces, and finally the surface under acidic attack using high concentration sulfuric acid (Table 1). For each case, five samples were prepared, and the selected two samples from five were used for the microscopic investigations.

2.2 Preconditioning prior to SEM

After the samples preparation regarding the surface condition in Table 1, they were dewatered by using 95-percent ethanol solutions and then kept dry naturally at room temperature. The samples were dried in a vacuum heater for 3 hours under the temperature of 100°C and vacuumed of approximately 1 N/m². Next, the samples were placed in a vacuum chamber until the pressure level reached 1 x 10⁻³ N/m². After that, they were stored in a vacuum desiccator under the pressure of 1 N/m² for two days. The final step included 60-second plasma-coating by Platinum and Palladium (Pt-Pd) using Hitachi's E-1030 ion sputter.

2.3 Scanning electron microscope, light-inverted optical microscope, and the image settings

We used an electron microscope model No. JXA-8200 by JEOL, an electron probe microanalyzer for SEM-EPMA. The JXA-8200 has a decent stage which allows the user to perform analysis of multiple samples at once. The machine is capable of x40 to x300,000 magnifications. We selected x100

magnification and used this value throughout the study as a control parameter. This magnification level generally governed the typical size of cement hydrate particles on the mortar surface. The image resolution of this machine is 1,280×1,024 pixels (1.2 megapixels), and the JXA-8200 can provide both SEI and BEI images. The acceleration voltage was set at 15 kV. The lens-to-object distance was kept between 10-12 mm.

As for the optical microscope, we used 'Eclipse Ti2', a light-inverted optical microscope by Nikon, with an integrated fixed lens of x100 magnification. This model is capable of capturing image resolution up to 10 megapixels. For consistency with the setting of the electron microscope, we also set the image resolution as 1.2 megapixels. All images were neatly taken with enough light support to ensure the image quality.

Sets of the surface image from the four cases were captured before and after preconditioning prior to SEM by light-inverted optical microscope. Later on, these optical images will be used for cross-comparison with another set of BEI and SEI images acquired from the electron microscopic investigation.

2.4 Analysis of microcracking on the surface and the effective area of Pt-Pd coating

By initial BEI image inspection, we found differences in microcracks among four cases. Thus the microcrack analysis shall be carried using an image analysis software, ImageJ with FIJI package. All BEI images were Kuwahara-filtered, applied threshold, binarized, and lastly skeletonized for acquiring information regarding microcrack amount and length [13], [14]. However, this method to obtain microcrack information is not suitable for the Case 2 in which the microcracks blended well with rough surface texture (Figure 1). Thus, the microcracking analysis was made among Case 1, 3, and 4. Also, an attempt on microcracking analysis of the image before preconditioning was also made but for an eligible study case only.

The coating area of Pt-Pd ions was investigated using surface images from the light-inverted microscope after the preconditioning step. Similar to the analysis of microcracking, the images were filtered, but applied a color threshold for silver, grey, and white zone instead (not concrete surface area). Thus, the area percentage of Pt-Pd coating was obtained. In addition, a microscopic photography technique called 'extended depth of field' was used in certain surface location to improve the optical image quality [15], [16]. The advantage of the mentioned technique is to minimize the focal loss on some surface images in Case 2 and 4 which contain

more significant variations in surface depth than that of the Case 1 and 3 specimens.

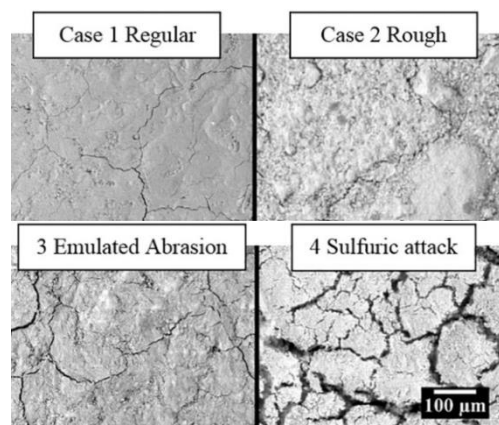


Figure 1 BEI images showing the surface condition of Case 1 to Case 4 in order from left to right

3. Results

Series of the representative optical image before and after preconditioning prior to SEM from Case 1 to 4 were provided in Figure 2. It can be claimed that the Pt-Pd coating effect is subjective to surface texture and its condition. The coating worked effectively on a flat surface (Case 1 and 3). Whereas, the surfaces containing rough textures and broader crack width (Case 2 and 4) had poorer Pt-Pd coating effect. Also, Case 4 had much broader surface crack width compared to other cases.

At x100 magnification, the quality of SEI and BEI images from four cases can be acceptable. However, the flashy white light was spotted in certain locations on the surface of Case 4 specimens while performing the analysis. The presence of flashy light indicated an insufficient conductivity and consequently leading to a terrible inaccuracy while performing an on-the-fly elemental analysis such as WDX and EDS.

The analysis indicated that microcracks on the surface in the three study cases were unequal. Also, the crack amounts before and after preconditioning prior to SEM immensely increased (See Table 2: Crack area ratio, Case 1 from <0.02% to 3.32% and Case 3 from nearly invisible to 1.32%). It was evident that microcracks suddenly appeared on the surface after preconditioning for that of the Case 1 and 3 specimens. The surface of the Case 4 specimens, which initially contained surface crack due to acidic attack, displayed a new additional set of microcrack, while the existing microcrack became significantly widened.

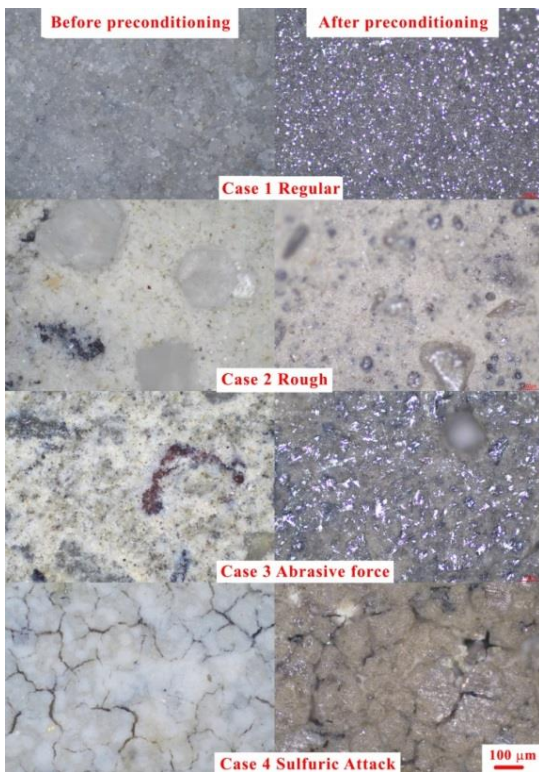


Figure 2 Surface conditions of case 1 to 4 before and after pre-conditioning prior to SEM (images obtained from the light-inverted optical microscope)

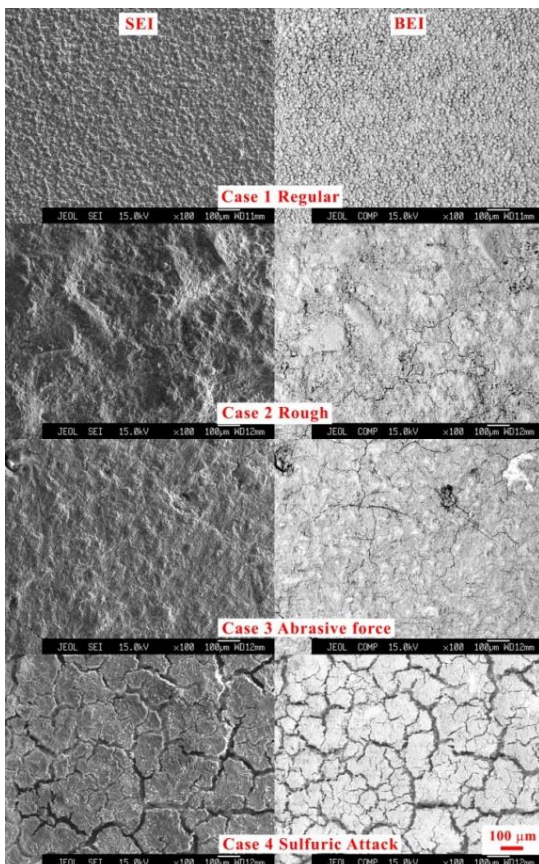


Figure 3 SEI and BEI images of concrete surface of the Case 1 to 4 capturing at the same location (each)

Table 2 Microcrack data before and after preconditioning prior to SEM at $\times 100$ (Total analysis area per image = $1,020,181 \mu\text{m}^2$)

Case No. (N=5)	Average crack length in total (μm)	Average crack width (μm)	Crack area ratio (%)
1 After	16,200	0.98	3.32
1 Before	N/A	N/A	<0.02
3 After	4,600	2.89	1.32
3 Before	N/A	N/A	N/A
4 After	23,200	10.47	23.73
4 Before	14,300	8.56	12.54

Note: Case 2 specimens were omitted from microcrack analysis

Table 3 Percentage of Pt-Pd coating area, Maximum zoom level with acceptable SEI and BEI image quality, and the eligibility to perform specific analysis

Case No.	Visual Pt-Pd coating area, N=5 (%)	Maximum zoom level with acceptable SEI and BEI image quality	On-spot WDX analysis accuracy, N=5 (%)	EPMA mapping analysis
1	95.4	3000 \times	76.4 (acceptable)	N/A
2	3.1	1500 \times	N/A	N/A
3	78.3	2000 \times	82.7 (acceptable)	N/A
4	15-6	750 \times	N/A	N/A

The percentage of visible Pt-Pd coating area and the highest magnification with acceptable image quality could be used to justify the quality effect of preconditioning. The visual Pt-Pd amounts indicate two hidden parameters which are surface smoothness and adequate amounts of conductivity. For this parameter, the surface of the Case 1 and 3 specimens showed a decent value in term of percentage coating. Furthermore, the maximum magnification with acceptable image quality reflects whether the surface conductivity is adequate or not. For Case 4 specimens, the result displayed the lowest acceptable magnification level of $\times 750$. This finding agreed well with the mentioned flashy light that was found on certain spot in SEI image of the Case 4 specimens. Also, the Pt-Pd percentage area from the case 2 specimens appeared off the league, but with considering the acceptable maximum zoom the value appeared valid (See Table 3, 1500 \times).

As for on-spot WDX analysis, the JXA-8200 required the user to adjust the Z value manually (object-to-lens distance). This parameter is immensely sensitive to height and consequently affects the measuring accuracy. For the unsmooth surface case, the user would undoubtedly experience difficulty in Z-value adjustment for the visual getting

from the optical microscope (OM) monitor is barely seen. Consequently, the on-spot WDX analysis on the case 2 and 4 specimens is therefore invalid due to the focal loss in detecting the reference point on the OM monitor. The average accuracy for on-spot WDX analysis for the Case 1 and 3 specimens was acceptable. This accuracy could be improved with additional grinding and polishing processes, but that is not suitable for this study. For the EPMA mapping, this analysis required much smoother surface. Practically, the surface must be smoothed and adequately polished. Thus, the EPMA mapping is not eligible for any case in this study for grinding and polishing are pre-requisite.

4. Discussion

4.1 Preconditioning effect on SEI and BEI images

In this study, we applied the same preconditioning treatment to four types of concrete surface, and we found that the quality image at higher magnification was not equal among the study cases. It can be suggested that one crucial factor is the degree of surface smoothness. The effects, therefore, appeared slightly stronger toward the SEI images, while the effect to BEI image could be considered marginal in the magnification range between $\times 40$ to $\times 750$. This range is sufficient for fundamental studies, which include detecting microcrack amounts, checking the property of mortar composition, and finding the particle size distribution of hydrated cement paste. However, for more sophisticated studies such as higher order of particle size distribution, and the shape study of hydrated cement paste in mortar, one attempt of practical preconditioning setting might not suffice for some particular surface conditions.

4.2 Preconditioning effect and surface microcracking

According to the literature, some scholars postulated that microcracking with the crack width lower than $10\text{-}12\ \mu\text{m}$ would be marginal regarding the chloride attack [17], [18]. However, it is the nature of research work that large portions of research papers prioritized on few specific parameters over the overall problems. The authors convinced that the microcracks with the crack width smaller than the threshold value, later on might cause a durability concern to concrete structures. In this study, the microcrack width of the Case 4 (acidic attack) specimens was approximately around the threshold level. Therefore, researchers should pay more attention to the effects of the pre-requisite step prior to the SEM analysis. We found that the surface crack width from the case with the influence of

preconditioning step (including vacuum heating and pressure changes) was approximately 20-30 percent larger than that from the case with no preconditioning step.

4.3 Preconditioning effect and microstructure of hydrated cement paste

Although this paper did not present any statistic result regarding this point, it still should be worthy noted that during specimen preparation step all samples were cured in water curing tanks. It was found that a flux layer of calcium hydroxide ($\text{Ca}(\text{OH})_2$) was formed coating the surface of mortar. Due to the vacuum-heating process causing thermal tolerances between the current and new layers, the $\text{Ca}(\text{OH})_2$ flux turned brittle and easily separated from the original surface (Figure 4). So, using the SEM-EPMA which is counted as one of the conventional SEM, might not be favorable for any supremely flat surface that was later on attached by another additional layer of crystalline flux. Also, we found that the acquiring information of the particle size distribution from the BEI images at the magnification level of $\times 100$ was surprisingly fit regarding the calcium hydroxide crystal morphologic study.

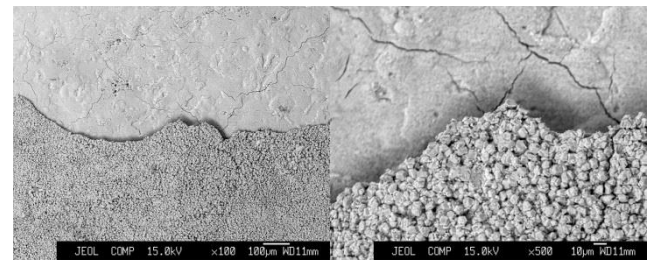


Figure 4 The BEI images from the case 1 specimen at $\times 100$ and $\times 500$ magnification level, showing the brittle calcium hydroxide flux (bottom) and the original surface of mortar (top)

5. Conclusion

In summary, this study focused on the preconditioning effect prior to SEM regarding three emulated surface deteriorations. The results showed an inconsistency of the conductive coating (Pt-Pd) among the four surfaces. In addition, the vacuum-heating process was found to alter the concrete surface in the cement hydrate region resulting in the increment of microcracking in all cases. Also, the existing microcrack prior to preconditioning became wider. This might lead to a misinterpretation of particular circumstances. Further investigation should focus on image analysis at higher magnification level ($\times 500$ or more), effects of vacuum-heating during the preconditioning step to concrete microstructure, and a proper Pt-Pd coating duration regarding the target surface types.

6. Acknowledgments

The author would like to thank Japanese government who provides funding for this research and also sponsors the Monbukagakusho (MEXT) Scholarship to the author for whole study periods in Tokyo Institute of Technology, Japan.

7. References

- [1] Z. hai He, S. gui Du, and D. Chen, "Microstructure of ultra high performance concrete containing lithium slag," in *J. Hazard. Mater.*, vol. 353, no. November 2017, 2018, pp. 35–43, doi: 10.1016/j.jhazmat.2018.03.063.
- [2] S. Cheng, Z. Shui, T. Sun, R. Yu, and G. Zhang, "Durability and microstructure of coral sand concrete incorporating supplementary cementitious materials," in *Constr. Build. Mater.*, vol. 171, 2018, pp. 44–53, doi: 10.1016/j.conbuildmat.2018.03.082.
- [3] H. Torbati-Sarraf and A. Poursaee, "Corrosion of coupled steels with different microstructures in concrete environment," in *Constr. Build. Mater.*, vol. 167, 2018, pp. 680–687, doi: 10.1016/j.conbuildmat.2018.02.083.
- [4] M. A. Coombes, L. A. Naylor, H. A. Viles, and R. C. Thompson, "Bioprotection and disturbance: Seaweed, microclimatic stability and conditions for mechanical weathering in the intertidal zone," in *Geomorphology*, vol. 202, 2013, pp. 4–14, doi: 10.1016/j.geomorph.2012.09.014.
- [5] T. Chlayon, M. Iwanami, and N. Chijiwa, "Durability of concrete structure with attached marine growth in tidal zone," in *Life-cycle of engineering systems: emphasis on sustainable civil infrastructure*, 2017, pp. 1202–1207.
- [6] M. A. Coombes, H. A. Viles, L. A. Naylor, and E. C. La Marca, "Cool barnacles: Do common biogenic structures enhance or retard rates of deterioration of intertidal rocks and concrete?," in *Sci. Total Environ.*, vol. 580, 2017, pp. 1034–1045, doi: 10.1016/j.scitotenv.2016.12.058.
- [7] J. Lv, J. Mao, and H. Ba, "Influence of marine microorganisms on the permeability and microstructure of mortar," in *Constr. Build. Mater.*, vol. 77, 2015, pp. 33–40, doi: 10.1016/j.conbuildmat.2014.11.072.
- [8] J. Lv, J. Mao, and H. Ba, "Influence of *Crassostrea gigas* on the permeability and microstructure of the surface layer of concrete exposed to the tidal zone of the Yellow Sea," in *Biofouling*, vol. 31, no. 1, 2015, pp. 61–70, doi: 10.1080/08927014.2014.999235.
- [9] T. Chlayon, M. Iwanami, and N. Chijiwa, "Combined protective action of barnacles and biofilm on concrete surface in intertidal areas," in *Constr. Build. Mater.*, vol. 179, 2018, pp. 477–487, doi: 10.1080/01621459.1952.10483441.
- [10] Y. Kawabata, E. Kato, and M. Iwanami, "Enhanced Long-Term Resistance of Concrete with Marine Sessile Organisms to Chloride Ion Penetration," in *J. Adv. Concr. Technol.*, vol. 10, no. 4, 2012, pp. 151–159, doi: 10.3151/jact.10.151.
- [11] P. P. Win, M. Watanabe, and A. Machida, "Penetration profile of chloride ion in cracked reinforced concrete," in *Cem. Concr. Res.*, vol. 34, no. 7, 2004, pp. 1073–1079, doi: 10.1016/j.cemconres.2003.11.020.
- [12] S. Sujjavanich, W. Wongcumchan, K. Waninthara, M. Sarikaphuti, and R. Kanthapong, "Investigation of alkali-silica reactivity potential of aggregate sources in the eastern part of Thailand [Thai translated]," in *J. Thail. Concr. Assoc.*, vol. 2, no. 2, 2015, pp. 1–9.
- [13] M. Ozen and M. Guler, "Assessment of optimum threshold and particle shape parameter for the image analysis of aggregate size distribution of concrete sections," in *Opt. Lasers Eng.*, vol. 53, 2014, pp. 122–132, doi: 10.1016/j.optlaseng.2013.08.020.
- [14] T. Chlayon, M. Iwanami, and N. (in press) Chijiwa, "Application of 2D micro-scale image analysis on concrete surface for evaluating concrete durability under various environments," in *Life-cycle of engineering systems: emphasis on sustainable civil infrastructure*, 2018.
- [15] B. Forster, D. Van De Ville, J. Berent, D. Sage, and M. Unser, "Complex wavelets for extended depth-of-field: A new method for the fusion of multichannel microscopy images," in *Microsc. Res. Tech.*, vol. 65, no. 1–2, 2004, pp. 33–42, doi: 10.1002/jemt.20092.
- [16] F. Aguet, D. Van De Ville, and M. Unser, "Model-based 2.5-D deconvolution for extended depth of field in brightfield microscopy," in *IEEE Trans. Image Process.*, vol. 17, no. 7, 2008, pp. 1144–1153, doi: 10.1109/TIP.2008.924393.
- [17] M. Maes, D. Snoeck, and N. De Belie, "Chloride penetration in cracked mortar and the influence of autogenous crack healing," in *Constr. Build. Mater.*, vol. 115, 2016, pp. 114–124, doi: 10.1016/j.conbuildmat.2016.03.180.
- [18] I. S. Yoon and E. Schlangen, "Experimental examination on chloride penetration through micro-crack in concrete," in *KSCE J. Civ. Eng.*, vol. 18, no. 1, 2014, pp. 188–198, doi: 10.1007/s12205-014-0196-9.